ACS APPLIED MATERIALS & INTERFACES

Research Article

www.acsami.org

# Polyviologen Hydrogel with High-Rate Capability for Anodes toward an Aqueous Electrolyte-Type and Organic-Based Rechargeable Device

Naoki Sano,[†] Wataru Tomita,[†] Shu Hara,[†] Cheong-Min Min,[‡] Jae-Suk Lee,[‡] Kenichi Oyaizu,[†] and Hiroyuki Nishide*[,†,‡]

[†]Department of Applied Chemistry, Waseda University, Tokyo 169-8555, Japan

[‡]Department of Nanobio Materials and Electronics, Gwangju Institute of Science and Technology, Gwangju 500-712, Korea

Supporting Information

**ABSTRACT:** A highly cross-linked polyviologen hydrogel, poly(tripyridiniomesitylene) (PTPM), has been designed as an anode-active material. It displays a reversible two-electron redox capability at −0.4 and −0.8 V vs Ag/AgCl in an aqueous electrolyte. The PTPM layer coated on a current collector by electropolymerization via a 4-cyanopyridinium electro-coupling reaction demonstrates a rapid charging-discharging reaction with a redox capacity comparable to that obtainable using the formula weight-based theoretical density, because of the combination of the redox-active viologen moieties built into the hydrogel. A test cell that has been fabricated using the developed PTPM anode, a poly(2,2,6,6-tetramethylpiperidinyloxy-4-yl acrylamide) (PTAm)-based cathode, and an aqueous electrolyte exhibits a discharging voltage of 1.1 and 1.5 V, and has proven its ability to be recharged more than 2000 times.

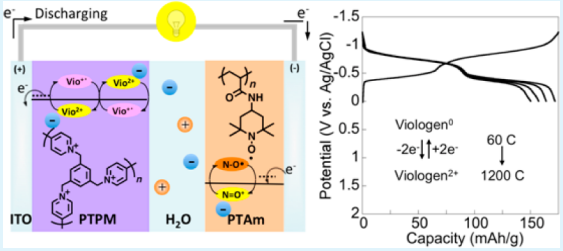


**KEYWORDS:** *rechargeable device, redox polymer, polyviologen, electropolymerization, aqueous electrolyte*

## INTRODUCTION

Organic-based and "wet-type" electric devices, which consist of organic materials and a liquid electrolyte to utilize electrode reactions that are characteristic of organic molecules, have come to play increasingly important roles to achieve rapid responses or large currents in sensors,[1] electrochromic displays,[2] solar cells,[3] and other electric devices. In one particular range of organic electronic devices, $\pi$-conjugated conducting polymers, wherein the electronic functionalities are expressed by the delocalized $\pi$-electrons as the carriers for electric conduction, have been greatly exploited as electro-active materials. Studies on the so-called "wet-type" devices, typified by batteries, have also been dependent on the use of $\pi$-conjugated polymers such as polyacetylene, polyaniline, polypyrrole, polythiophene, and polyphenylene.[4] However, the slow kinetics of their electrode reactions in a liquid electrolyte due to the presence of intermolecular interchain electron transfer processes often limit the rates of electrochemical response or charging/discharging.

Hydrogels,[5] which embed water molecules in cross-linked structures or polymer chain random coils, have been paid considerable attention not only in the field of biochemistry (e.g., cell culture, drug delivery, and soil amendment)[6] but also in the field of electrochemistry.[7−10] Their high electrochemical mobility of molecules and/or ions allows their use as electric media such as ion-exchange films, hole-conductive materials, and gel electrolytes in fuel cells,[8] solar cells,[9] and secondary batteries.[10]

Recently, we reported that redox polymer gels bearing robust and redox-active radical pendant groups, which we called "radical polymers," possessed the advantages of both liquid and solid phases to enable high electron diffusion and high radical concentration.[11] We also utilized the radical polymers as electrode-active materials, which could store and supply electrons at a high speed in organic rechargeable batteries.[12] Moreover, we reported hydrophilic radical polymers as cathode-active materials for organic batteries with aqueous electrolytes, which possessed a high equivalent electrical conductivity (on the order of $10^{-2}$−$10^{-3}$ S m$^2$ mol$^{-1}$), and displayed very fast charging/discharging characteristics at 3 s (1200 C).[13] These results indicated that the amorphous polymer layers with aliphatic (i.e., nonconjugated) main chains allow electrolyte anions to penetrate into the layer with aqueous electrolytes and enhance the electron self-exchange reactions.[14] However, to develop the new generation of organic rechargeable batteries, anode-active materials that exhibit high-energy density, high-power density, and redox reactions at negative potentials in aqueous electrolytes are required.

In search of a nonconjugated chain bearing the *n*-type redox sites, we focused on viologen derivatives ($V^{2+}$) based on the following characteristics: (i) the two-electron reaction for the ultimate charging ($V^{2+}$ + 2e$^-$ = $V^0$), which allows the charge

Received: November 9, 2012
Accepted: January 24, 2013
Published: January 24, 2013

 © 2013 American Chemical Society 

storage with two organic heterocycles and leads to an inherently large storage density,[15] (ii) the robustness of the cation radical state ($V^+$) and the neutral state ($V^0$) in solutions and/or gels in the well-known repeatable electrochromic devices,[16] and (iii) the suitable redox potentials in the range of −0.4 V to −1.0 V vs Ag/AgCl. The *n*-type redox activity of viologen derivatives could provide an output voltage (equal to the potential gap) of more than 1.0 V during the fabrication of cells with *p*-type cathode-active materials such as poly(2,2,6,6-tetramethylpiperidinyloxy-4-yl acrylamide) (PTAm) and poly-(2,2,6,6-tetramethylpiperidinyloxy-4-yl vinylether) (PTVE) with redox potentials at approximately 0.7 V vs Ag/AgCl.[13,17] Moreover, viologen polymers immobilized on a current collector have been reported to be synthesized via electropolymerization, using the reductive coupling reaction of 4-cyanopyridinium moieties (i.e., the coupling of two 4-cyano-1,4-dihydropyridinium radicals, accompanied by the elimination of two cyanides, as shown in Scheme 1).[18,19]

**Scheme 1. Reductive Coupling Reaction of 4-Cyanopyridinium Moieties[14,17]**

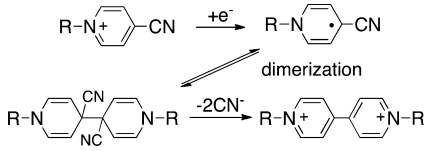


This electropolymerization is suitable for electrode-active materials because (i) not only insoluble but also swellable polymers are synthesized on a current collector easily and (ii) viologen units in the synthesized polymers are nonconjugated and transport electrons rapidly through a hopping reaction between viologen sites. In other studies, the viologen polymer electrodes are prepared by the substitution to polyalkylhalogen side chains, surface modification using graft reactions,[20] layer-by-layer assemblies,[21] and polyion complex formation with anionic polymers,[16b,22] resulting in capacities lower than their theoretical or formula weight-based densities and low rate performances due to the limited mass-transfer process.

In this paper, we report, for the first time, the excellent charge storage properties of poly(tripyridiniomesitylene) (PTPM), which is a new organic electrode-active material (Scheme 2). PTPM was designed by a highly cross-linked

**Scheme 2. Molecular Structures of PTPM and PTAm[16]**

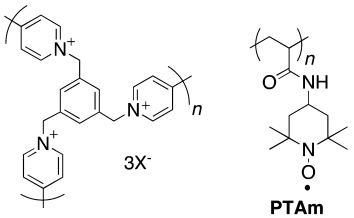


**PTPM** 3Cl⁻: 175 mAh/g

polyviologen that has a considerable number of viologen moieties per unit to fulfill the following purposes: (i) high charging-discharging capacity (theoretical redox capacity = 175 mAh $g^{-1}$) ascribed to the stoichiometric two-electron redox reaction, (ii) high charging-discharging rate resulting from the rapid electron transfer process of each viologen unit, and (iii) long cycle life derived from the chemical stability of the redox reaction and from the amorphous gels (Scheme 3). An important aspect of the electrochemistry of the redox process of PTPM is the unprecedented reversible and rapid electrochemistry of the two-electron redox reaction of the viologen sites in aqueous media. A totally organic-based rechargeable device was fabricated using PTAm as the cathode-active material and an aqueous electrolyte of NaCl. We also describe, toward an environmentally benign future technology, the advantages of an aqueous electrolyte-based and organic polymer PTPM/PTAm-based rechargeable battery.

## EXPERIMENTAL SECTION

**Materials.** 4-Cyanopyridine and sodium chloride were obtained from Tokyo Kasei Co. 1,3,5-Tris(bromomethyl)benzene was obtained from Aldrich Co. All solvents were purified by distillation prior to use. All other reagents were obtained from Kanto Chemical Co. and were used without further purification. The indium tin oxide (ITO) substrate was purchased from Asahi Glass Co. and cleaned by plasma etching prior to use. A porous substrate was prepared through a 450 °C sinter of the ITO nanoparticles (20 nm) in an aqueous dispersion with poly(ethylene glycol) (PEG, $M_n$ = 14 000) coated on an ITO electrode.

**Apparatus.** $^1$H and $^{13}$C NMR spectra were recorded on a JEOL Model JNM-LA500 spectrometer with chemical shifts downfield from tetramethylsilane (TMS) as the internal standard. Infrared spectra and UV−vis spectra were obtained using a Nicolet Model 6700 spectrometer and a Jasco Model V-670 spectrometer. Mass spectra were obtained using a JEOL Model JMS-SX102A spectrometer or a Shimadzu Model GCMS-QP5050 spectrometer. Elemental analyses were performed using a Perkin−Elmer Model PE-2400 II elemental analyzer and a Metrohm Model 645 multi-DOSIMAT auto buret. Two parallel analyses were performed for each sample. Morphological changes of PTPM layer were observed by a KLA Tencor P-15 contact stylus profiler and scanning electron microscopy (SEM). A preliminary microscopic analysis was performed using a laser-scanning microscope (KEYENCE, Model VK-9700) as a method of noncontact thickness measurement, with the resolution of 1 nm. The water droplet contact angle was measured with a drop shape analysis system (KRÜSS, Model DSA100).

**Synthesis of 1,3,5-Tris(4-cyanopyridinio)mesitylene (TPM) Bromide Salts.** 1,3,5-Tris(bromomethyl)benzene (4.5 g, 12.5 mmol) and 4-cyanopyridine (13.0 g, 125.0 mmol) were refluxed in acetonitrile (40 mL) for 24 h under nitrogen. The resulting yellow-colored bromide salt was recovered by filtration, washed with acetonitrile, and recrystallized from methanol/ethanol to yield yellow needlelike crystals. This afforded 7.3 g of the final product (yield = 85%). $^1$H NMR $\delta_H$ ($D_2O$, 500 MHz, ppm, TMS): 9.10 (d, 6H, *α-H* of pyridinium), 8.41 (d, 6H, *β-H* of pyridinium), 5.99 (s, 6H, $CH_2$), 2.19 (s, 3H, ph). $^{13}$C NMR $\delta_C$ ($D_2O$, 500 MHz, ppm, TMS): 147.0, 135.5, 133.2, 132.6, 129.8, 115.1, 65.3. Anal. Calcd for $C_{27}H_{21}Br_3N_6$: C, 48.5%; H, 3.2%; N, 12.6%. Found: C, 48.2%; H, 3.1%; N, 12.4%. FAB-MS: *m*/*z* = 226.4, calcd for 223.1.

**Preparation of Poly(2,2,6,6-tetramethylpiperidine-4-yl acrylamide) (PTAm) Electrode.** Poly(2,2,6,6-tetramethylpiperidine-4-yl acrylamide) (PTAm) was synthesized with reference to our previous report[17] ($M_w$ = 1.1 × 10$^6$, $M_w/M_n$ = 2.3, radical concentration = 96%, formula-weight-based capacity = 119 mAh $g^{-1}$ (× 0.96)). The THF solution of PTAm (10−50 g $L^{-1}$) was spin-coated on an ITO substrate using a MIKASA Model 1H-D3 spin coater at 1000−6000 rpm, and dried in vacuum for 12 h to give a thin-layer electrode. The layer thickness was estimated, using a KLA Tencor P-15 contact stylus profiler, to be 100−200 nm.

**Electrochemical Measurements.** Electrochemical measurements (cyclic voltammogram, chronoamperometry, chronocoulometry, and chronopotentiometry) were performed using an ALS electrochemical analyzer (BAS, Inc., Model 660D). All measurements were performed under an atmosphere of argon. A one-component cell with an ITO glass substrate (2.5 cm × 2.5 cm), a platinum wire, and an Ag/AgCl electrode as the working electrode, the counter electrode, and the

**Scheme 3. Schematic Illustration of a Network Structure in the PTPM Layer**

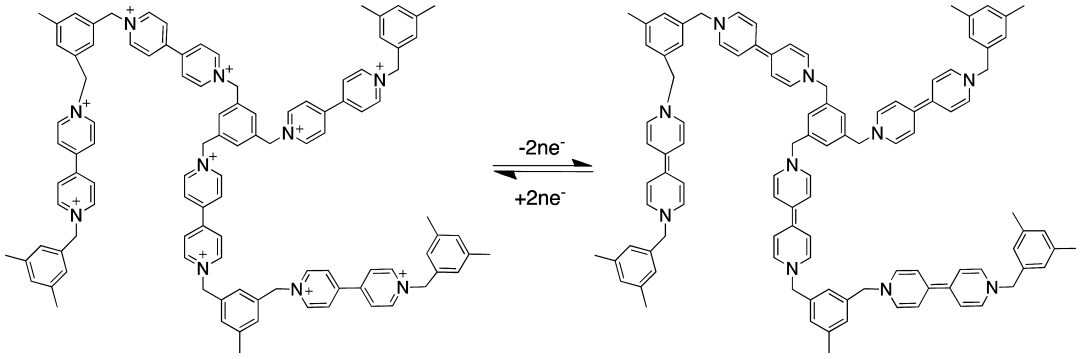


reference electrode, respectively, were employed to obtain the voltammograms. Aqueous electrolytes were prepared using deionized water after distillation.

CA measurement:

$$i_t = nFAC\left(\frac{D}{\pi t}\right)^{1/2} \quad (1)$$

where $i_t$, $n$, $A$, $C$, $D$, and $t$ are the current, numbers of electrons, the geometrical surface of the ITO electrode, the concentration of the pendant viologen group, the diffusion constant for the charge propagation, and the time, respectively.

Electrochemical quartz crystal microbalance (EQCM) was performed using a potentiostat system (Model ALS660B) connected with the crystal resonator chemistry measurement system (SEIKO EG&G Co., Model QCA922). EQCM were measured with a three-electrode beaker cell using the glassy carbon QCM electrode (SEIKO EG&G Co., Model QA-A9MC(M)) as the working electrode. The change in the resonant frequency ($\Delta f$) measured simultaneously with the cyclic voltammograms was recorded in the potential range between 0 and −1.2 V, at a scan rate of 5 mV $s^{-1}$. The change in mass ($\Delta m$), accompanied by the reduction of the polymer layer, was determined by employing Sauerbrey's equation (eq 2):

$$\Delta f = -2f_0^{\,2}A^{-1}(\rho_q\mu_q)^{-1/2}\Delta m \quad (2)$$

where $f_0$ is the fundamental frequency of the QCM ($f_0$ = 9.1 MHz), $A$ the electrode area ($A$ = 0.196 $cm^2$), $\rho_q$ the density of quartz ($\rho_q$ = 2.65 g $cm^{-3}$), and $\mu_q$ the shear modulus of quartz ($\mu_q$ = 2.95 × $10^{11}$ dyn $cm^{-1}$ $s^{-2}$).

An impedance spectrum analyzer (Solartron, Model SI 1260) with ZPlot software was employed to measure the AC impedance of three types of half-cells composed of a PTPM layer and the respective electrolytes. The resistance of the charge transfer ($R_{CT}$) was calculated with ZPlot software, relative to the diameter in high-frequency region, by referring to a previous paper.[23] The AC potential amplitude was set at 10 mV and the frequencies ranged from 0.01 Hz to 10 000 Hz.

AC impedance analysis:

$$R_L = \left(\frac{1}{C_L}\right)\frac{L^2}{3D} \quad (3)$$

where $R_L$ is the low-frequency polymer resistance, $C_L$ the low-frequency polymer redox capacitance, $L$ the polymer layer thickness, and $D$ the diffusion constant for the charge propagation.

The formula-weight-based theoretical density (or capacity) (in mAh $g^{-1}$) was calculated according to 1000 $nFM^{-1}$ $(3600)^{-1}$, where $n$, $F$, and $M$ are stoichiometric number of electrons, the Faraday constant, and the molar mass of the repeating unit, respectively. The $n$ value was 1.5 and 1.5 both in the first and second redox reaction ($V^{2+}/V^{+\bullet}$ and $V^{+\bullet}/V^0$), per repeating units of PTPM. The redox capacity (in mAh $g^{-1}$) was obtained employing 1000 $Qm^{-1}$ $(3600)^{-1}$, where $Q$ and $m$ are, respectively, the charge passed in electrolysis and the loading weight of the anode-active material calculated with the layer thickness under dry conditions.

**Cell Fabrication and Charging/Discharging Test.** A half cell composed of the PTPM layer on an ITO substrate in a beaker cell was charged and discharged at the current density of 120 C (21 A $g^{-1}$) repeatedly up to 5000 cycles. The "1 C-rate" is defined as the current density at which the charging or discharging of the cell takes 1 h. A totally organic-based battery was fabricated using the PTPM layer with a thickness of 100 nm as the anode, a PTAm layer with a thickness of 200 nm as the cathode, and 0.1 M NaCl aqueous electrolyte under argon atmosphere. Charging/discharging capacity and output voltage of the cell were tested by chronopotentiometry at the current density of 120 C (21 A $g^{-1}$). Cycle performance of the cell was examined by repeating charging/discharging galvanostatic cycles at 120 C (21 A $g^{-1}$). The cutoff voltage of the PTAm cathode was 0.3 and 1.9 V (vs PTPM anode), by considering potential windows of the electrolyte such as the oxidation of the chloride anion.

## RESULTS AND DISCUSSION

Figure 1 shows the multiple-scanned cyclic voltammogram obtained for a 0.02 M TPM bearing three cyanopyridinium

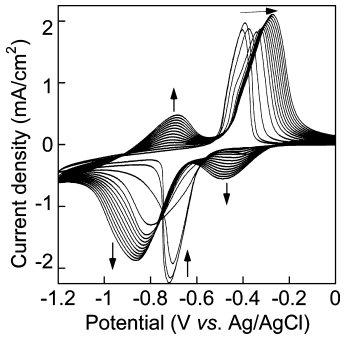


**Figure 1.** Cyclic voltammogram of the TPM on an ITO substrate during the course of the electropolymerization in a 0.1 M NaCl aqueous solution at a scan rate of 50 mV $s^{-1}$ (15 scan cycles).

moieties in aqueous 0.1 M NaCl in the range of 0 to −1 V (vs Ag/AgCl). The reduction peak at −0.72 V decreased; the reduction peaks at −0.86 and −0.49 V and the oxidation peaks at −0.74 V increased in terms of the peak currents; and the oxidation peak at −0.41 V slid to −0.25 V during the continuous scans, where the viologen moieties on ITO were formed by the cyanopyridinium moieties. The PTPM anodes (50, 100, and 200 nm thickness) were prepared by the reductive electropolymerization of the TPM through constant potential electrolysis at −0.75 V (vs Ag/AgCl) on an ITO substrate (with a dipping area of 2.0 cm × 2.5 cm) for 500, 1000, and 2000 s, respectively, where the cyanopyridinium

moieties of the TPM were reduced to form the viologen moieties (the reduction potential of cyanopyridinium = −0.68 V). After the electropolymerization, a dark purple obscure layer appeared around the surface of the ITO substrate in the TPM, and a slightly yellow layer in the dry state was formed on the ITO substrate. The layer was insoluble in water and common organic solvents, which revealed that the polymeric product on the ITO substrate possessed a highly cross-linked structure derived from the multiarmed monomeric structure.[18] The topographic chart measured by a contact stylus profiler shows that the surface of the PTPM layer was pinhole-free and smooth (surface roughness of <5 nm). The SEM image (cross-sectional structure; see Figure 2) shows that the PTPM layer possessed a homogeneous and nanometer-scale pinhole-free configuration inside the layer.

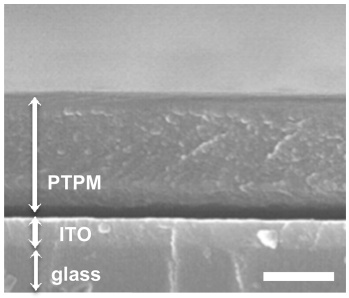


**Figure 2.** SEM image of the cross section of the electropolymerized PTPM layer on an ITO substrate. Scale bar = 100 nm.

Figure 3 shows that the layer thickness (denoted in the figure by solid circles, ●) in the range of 50−320 nm under a drying

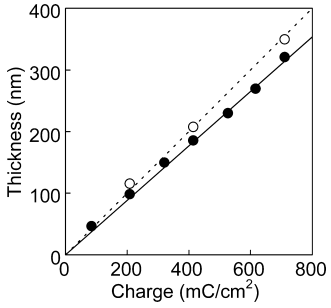


**Figure 3.** PTPM layer thickness (●) in the dry state and (○) in the 0.1 M NaCl solution, versus the charge passed during the reductive electropolymerization.

condition corresponded to the charge amount passed during electropolymerization. A preliminary microscopic analysis of the polymer volume before and after the swelling in water indicated that the degree of swelling under equilibrated conditions was ca. 1.3 (v/v), which corresponded to the increase of only 10% in the thickness under a swelling condition (denoted by open circles, ○) and suggested that the high site concentration was maintained in the swollen layer, because of the highly cross-linked structure. The static water contact angle of the PTPM layer on ITO was <5°, which is categorized as "super-hydrophilic", by virtue of the high concentration of viologen moieties on the surface, and is significantly smaller than the angle of 15°−30° for the surface of the viologen-grafted substrate[20] and the regular general polyviologen electrode, PV10-PSS spin-coated on ITO.[16b]

In the Fourier transform infrared (FT-IR) measurement, the spectra of the polymeric product showed a decrease in the intensity of the CN group peak ($\nu$ = 2244 $cm^{-1}$) down to <5%, implying that most of the cyanopyridinium moieties were consumed during the polymerization (see Figure S1 in the Supporting Information). The UV−vis spectra of the polymeric product under application of the reductive potential at −0.85 V vs Ag/AgCl gave increases in the absorption at 380 nm and of a broad band in the region of 500−600 nm ascribed to the produced viologen cation radical moieties (Figure S2 in the Supporting Information).

The PTPM layer showed reversible two-step redox waves at −0.48 and −0.86 V repeatedly in a monomer-free 0.1 M NaCl aqueous solution, derived from the redox reaction of the viologen moieties. This result suggests that the polymer has a viologen structure resulting from the electropolymerization of the 4-cyanopyridinium moieties. These two redox potentials of the PTPM layer were slightly higher than those of the conventional viologen derivatives, such as methylviologen[14] and liner polyviologens,[16] probably because the viologen moieties of the PTPM network could prevent the dimer ($V_2^{2+}$ or $V_2^{0}$) formation of the cation radical state ($V^+$) or the neutral state ($V^0$) through a radical−radical interaction or $\pi-\pi$ stacking and result in stabilization of the one- or two-electron-reduced viologen moieties. The redox waves also show a narrow peak-to-peak separation ($\Delta E_1$ = 40 mV, $\Delta E_2$ = 137 mV) for the layer with a thickness of 40 nm, indicating the electrochemically reversible and very fast electron transfer within the polymer layer.

The cyclic voltammetric EQCM measurement revealed the mass change of the compensating anions and the accompanying water molecules into the layer during the redox reaction (Figure 4). The frequency changes were converted into mass

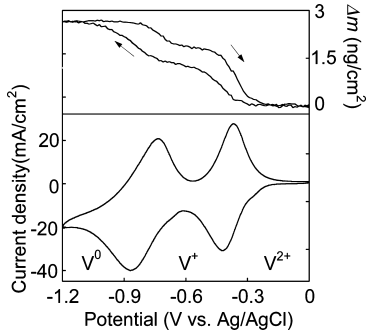


**Figure 4.** Cyclic voltammogram and mass change ($\Delta m$) in EQCM of the 50-nm-thick PTPM layer on an Au electrode in the 0.1 M NaCl aqueous solution at scan rate of 50 mV $s^{-1}$.

changes using the Sauerbrey equation (see eq 2). During the mass change, the PTPM layer released the anions in the two steps during the reduction from the $V^{2+}$ to $V^0$ state and returned to its original value after the oxidation; the layer showed a reversible and repeatable mass change in several redox cycles. The mass changes relative to the redox capacity ($\Delta mFQ^{-1}$) were 80 g $mol^{-1}$, suggesting that the counteranion incorporation into the layer was accompanied by 2.5 $H_2O$ molecules (calculated using the following equation: $(\Delta mF\tilde{Q}^{-1} - M_{anion})/M_{H_2O}$).[24]

The charge propagation process in the PTPM layer was analyzed with potential-step chronoamperometry, using Cottrell plots and an AC impedance analysis, separately (see Figure

5 and Table 1), assuming a semi-infinite diffusion at the early stage of the electrolysis. In the CA measurement, the slope

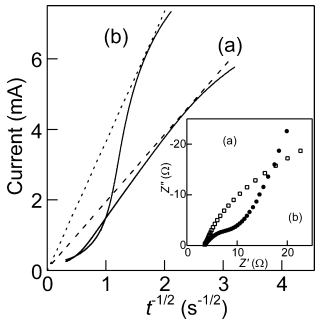


**Figure 5.** Cottrell curves for chronoamperometry of the PTPM layer on an ITO substrate after applying a potential pulse from 0 to (a) −0.7 V and (b) −1.1 V vs Ag/AgCl in a 0.1 M NaCl aqueous solution. Inset shows the impedance spectra for the charge propagation process of the PTPM layer during constant potential electrolysis at (a) −0.48 V and (b) −0.86 V.

**Table 1. Electrochemical Parameters of Redox Polymer Electrodes**

| | | Diffusivity, $D$ ($\times 10^{-10}$ cm$^2$ s$^{-1}$) | | |
|---|---|---|---|---|
| electrode | $E_{1/2}$ (V) | CA measurement | AC impedance measurement | $R_{CT}$[a] (Ω) |
| PTPM | −0.48 | 2.4 | 1.3 | 26 |
| PTPM | −0.86 | 8.9 | 7.2 | 10 |
| PTAm | +0.66 | 1.2 | 0.8 | 32 |

[a]Via AC impedance measurement.

obtained for the second redox reaction ($E_{1/2}$ = −0.86 V, $V^+/V^0$) of the PTPM layer was larger than that obtained for the first redox reaction ($E_{1/2}$ = −0.48 V, $V^{2+}/V^+$) of the PTPM layer. In the AC impedance analysis, the diameter of the semicircle ascribed to the resistance of charge transfer ($R_{CT}$) for the second redox reaction of the PTPM layer was smaller than that for the first redox reaction of the PTPM layer. These results suggest that the charge diffusion for the second redox reaction ($V^+/V^0$) of the PTPM layer was considerably faster than that for the first redox reaction ($V^{2+}/V^+$). The volume change in the second redox reaction (attributed to the accompanying $H_2O$ molecules: $n_{red}$ = 1.2; $n_{ox}$ = 0.9) was fewer than that in the first reaction ($n_{red}$ = 1.3, $n_{ox}$ = 1.6), particularly for the oxidation process, as estimated by the mass change during each redox reactions (Figure 4). The average diffusion coefficient ($D$) of the PTPM layer for the two-step redox reaction exceeded that of the PTAm cathode-active material (Table 1) and the conventional polyviologen electrodes, such as PV10-PSS spin-coated on an ITO substrate ($D$ = 0.9 × $10^{-10}$ cm$^2$ s$^{-1}$).

The charging-discharging curves for the half-cell composed of the PTPM layer as the working electrode in aqueous 0.1 M NaCl exhibited a two-step plateau voltage near −0.39 V to −0.51 V and −0.77 V to −0.96 V (vs Ag/AgCl), which agreed with the redox potential of the PTPM layer (−0.48 V and −0.86 V), as shown in Figure 6. The charging discharging capacities almost coincided at 174 mAh g$^{-1}$ with the Coulombic efficiency of >95% (discharging capacity over the charging capacity) under rapid charging−discharging at a high C-rate of 60 C. Note that most conventional batteries function in the charging or discharging mode at 1 C that takes 1 h. With respect to the discharging rate performance, Figure 6 revealed

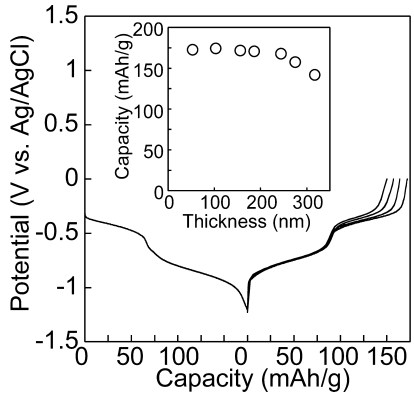


**Figure 6.** Charging and discharging curves of a half cell of PTPM anode at various discharging rates of 10.5, 21, 105, and 210 A g$^{-1}$ (60—1200 C) in a NaCl aqueous solution. The PTPM layer was 80 nm thick. Inset shows the discharging capacity versus layer thickness of the PTPM layer on an ITO substrate.

that the discharging capacity of 150 mAh g$^{-1}$ (86% versus the calculated capacity) was maintained even with the rapid charging at 1200 C and showed the decrease in the discharging capacity during the first redox reaction ($V^+/V^{2+}$) mainly, which was supported by the result of the diffusion constant for the charge propagation (see Table 1). In the dependence of the discharging capacity on the layer thickness, 250 nm of the PTPM layer displayed an output discharging capacity of >170 mAh g$^{-1}$, because of the high concentration of viologen units in the PTPM layer leading to an efficient electron-hopping reaction. Moreover, the advantage of PTPM is the capability of preparing an ultrathin layer on the surface of a submicrometer-ordered porous substrate by the method of electropolymerization (see Figure S4 in the Supporting Information). Figure S4 shows that the PTPM layer (<10 nm) was coated on the porous substrate with nanometer-ordered roughness. This electrode allows outputting the stoichiometric capacity at a high-rate charging−discharging performance, even when the PTPM layer thickness is expressed in micrometers.

The cycling performance of the charging−discharging at cutoff voltages of 0 to −1.2 V and a C-rate of 60 C is also shown in Figure 7. Even after 5000 charging−discharging cycles, the PTPM anode was maintained at almost 90%, with the Coulombic efficiency of 85%, indicating that the highly

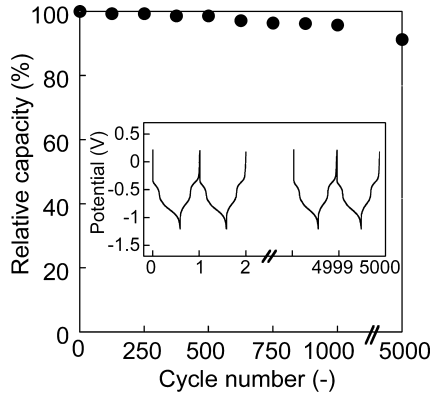


**Figure 7.** Cycle performance of PTPM, with respect to discharging capacity. Inset shows the charging and discharging curves of PTPM, in an aqueous NaCl solution at a current density of 21 A g$^{-1}$, with a layer thickness of 80 nm.

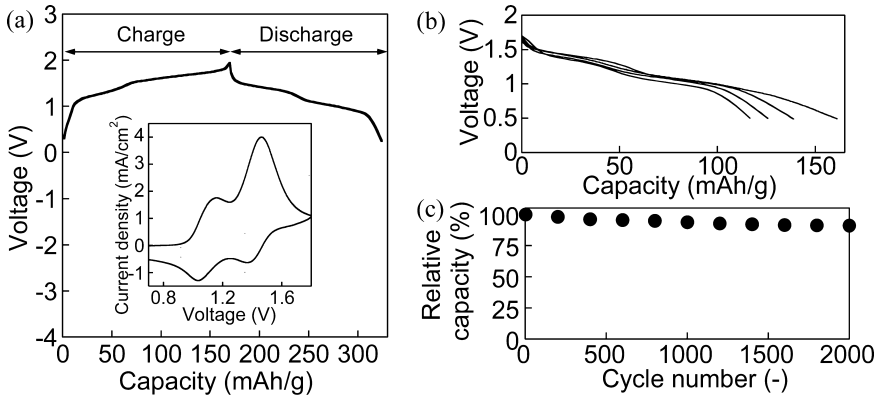


**Figure 8.** (a) Charging and discharging curves of the PTPM/PTAm cell with an aqueous NaCl electrolyte at 5 A $g^{-1}$ (60 C) (inset shows a cyclic voltammogram of the PTPM/PTAm cell at a scan rate of 50 mV $s^{-1}$). (b) Discharging curves of the PTPM/PTAm cell with the aqueous NaCl electrolyte at various discharging rates of 21, 42, 105, and 210 A $g^{-1}$ (120—1200 C). (c) Cycle performance of the PTPM/PTAm cell, with respect to discharging capacity.

cross-linked structure of the PTPM layer allowed the layer to stay on the ITO substrate without elusion or exfoliation into the electrolyte during the electrolysis, and that the charged species, the quinoid structure of PTPM, stoichiometrically contributed to the following discharging process.

To evaluate its anode performance in a full cell, a test cell was fabricated with a PTPM layer anode, a poly(2,2,6,6-tetramethylpiperidine-4-yl acrylamide) (PTAm) layer cathode, and aqueous 0.1 M NaCl. PTAm was selected as a suitable cathode for coupling with the PTPM, because PTAm displays a reversible redox at 0.66 V (vs Ag/AgCl) in an aqueous electrolyte. The test cell, which was composed of the PTAm cathode and the PTPM anode, outputted a voltage of more than 1.0 V, revealing the potential gap between the PTAm and PTPM mentioned in our previous reports.[17,24] The charging–discharging curves of the fabricated cell displayed a two-step plateau voltage at 1.14 and 1.52 V, which agreed with the calculated output voltage at the redox potentials of −0.48, −0.86, and 0.66 V (vs Ag/AgCl) for PTPM and PTAm, respectively. The discharging capacity of 165 mAh $g^{-1}$ agreed with the calculated capacity for the two-electron reaction of PTPM. With respect to the discharging rate performance, the test cell maintained a discharging capacity of 110 mAh $g^{-1}$ (63% vs the calculated capacity) even with the tremendously rapid charging at 1200 C and shows the decrease in the discharging capacity of the PTPM anode at the first redox reaction ($V^{+}/V^{2+}$) mainly (Figure 8). The cycling performance of the charging–discharging at the cutoff voltages of 0.3–2.0 V and the C-rate of 60 C is shown in the inset in Figure 8. After 2000 cycles, the discharging capacity was maintained at more than ca. 80% of the initial capacity, exhibiting the long cycle life of the battery. These results indicated that the utilization of PTPM anode for aqueous electrolyte-based rechargeable batteries allowed high-rate charging–discharging and long cycle performance.

## CONCLUSIONS

A highly cross-linked polyviologen hydrogel, poly(tripyridiniomesitylene) (PTPM), was synthesized and characterized as a hydrophilic and electrode-active polymer. The PTPM layer, even with a thickness in the order of submicrometers, coated on a current collector and equilibrated with an aqueous NaCl solution showed a reversible redox capacity in agreement with that calculated on the basis of the layer thickness. Hence, it could be concluded that the PTPM layer was defect-free for the two-electron redox process of the viologen moiety and was homogeneously solvated with the aqueous electrolyte. A half cell containing a PTPM electrode showed a very-rapid charging–discharging performance based on the combination of the hydrophilic radical polymer and the aqueous electrolyte, possessing high electrical conductivity. A full cell fabricated with a PTPM polymer anode, a PTAm cathode, and an aqueous electrolyte displayed reversible charging–discharging curves at the output voltage of 1.1 and 1.5 V and a cycle performance of >2000 cycles. A combination of organic-based polymer cathode and anode, and aqueous electrolyte, could ensure both an ideal and environmentally benign design and a rapid charging/discharging performance and long cycle life.

## ASSOCIATED CONTENT

### Supporting Information

Additional information (Figures S1–S4) as noted in the text. This material is available free of charge via the Internet at http://pubs.acs.org.

## AUTHOR INFORMATION

### Corresponding Author

*E-mail: nishide@waseda.jp.

### Notes

The authors declare no competing financial interest.

## ACKNOWLEDGMENTS

This work was partially supported by Grants-in-Aid for Scientific Research (Nos. 24750113 and 24225003) and the Global COE program at Waseda University from MEXT, Japan, and the World-Class University (WCU) program at GIST through a grant (Project No. R31-2008-000-10026-0) provided from MEST, Korea.

## REFERENCES

(1) (a) Park, M.-K.; Deng, S.; Advincula, R. C. *J. Am. Chem. Soc.* **2004**, *126*, 13723–13731. (b) Thomas, S. W.; Joly, G. D.; Swager, T. M. *Chem. Rev.* **2007**, *107*, 1339–1386.

(2) (a) Beaujuge, P. M.; Reynolds, J. R. *Chem. Rev.* **2010**, *110*, 268–320. (b) Vasilyeva, S. V.; Unur, E.; Walczak, R. M.; Donoghue, E. P.; Rinzler, A. G.; Reynolds, J. R. *ACS Appl. Mater. Interfaces* **2009**, *1*, 2288–2297.

(3) (a) O'Regan, B.; Grätzel, M. *Nature* **1991**, *353*, 737−740. (b) Fang, Z.; Eshbaugh, A. a; Schanze, K. S. *J. Am. Chem. Soc.* **2011**, *133*, 3063−3069.
(4) Novák, P.; Müller, K.; Santhanam, K. S. V.; Haas, O. *Chem. Rev.* **1997**, *97*, 207−281.
(5) In the previous papers,[25] hydrogels are defined to possess the amount of water from 10% to thousands of times of the weight of the xerogel. The highly cross-linked polyviologen, poly(tripyridiniomesitylene) (PTPM), uptook ca. 30% water under the equilibrated condition and was called as a hydrogel in this paper.
(6) (a) Shimizu, T.; Yamato, M.; Kikuchi, A.; Okano, T. *Biomaterials* **2003**, *24*, 2309−2316. (b) Qiu, Y.; Park, K. *Adv. Drug Delivery Rev.* **2001**, *53*, 321−339. (c) Friedman, M. *J. Agric. Food Chem.* **2003**, *51*, 4504−4526.
(7) Guiseppi-Elie, A. *Biomaterials* **2010**, *31*, 2701−2716.
(8) Lee, K.; Jeong, M.; Lee, J.; Lee, J. *Macromolecules* **2009**, *42*, 584−590.
(9) Sakaguchi, S.; Ueki, H.; Kato, T.; Kado, T.; Shiratuchi, R.; Takashima, W.; Kaneto, K.; Hayase, S. *J. Photochem. Photobiol. Chem.* **2004**, *164*, 117−122.
(10) Stephan, M. *Eur. Polym. J.* **2006**, *42*, 21−42.
(11) Oyaizu, K.; Nishide, H. *Adv. Mater.* **2009**, *21*, 2339−2344.
(12) (a) Nishide, H.; Oyaizu, K. *Science* **2008**, *319*, 737−738. (b) Oyaizu, K.; Ando, Y.; Konishi, H.; Nishide, H. *J. Am. Chem. Soc.* **2008**, *130*, 14459−14461.
(13) Koshika, K.; Sano, N.; Oyaizu, K.; Nishide, H. *Chem. Commun.* **2009**, 836−838.
(14) Koshika, K.; Sano, N.; Oyaizu, K.; Nishide, H. *Macromol. Chem. Phys.* **2009**, *210*, 1989−1995.
(15) Monk, P. M. S. *The Viologens*; John Wiley & Sons, Ltd.: Chichester, U.K., 1999.
(16) (a) DeLongchamp, D. M.; Kastantin, M.; Hammond, P. T. *Chem. Mater.* **2003**, *15*, 1575−1586. (b) Takahashi, Y.; Hayashi, N.; Oyaizu, K.; Honda, K.; Nishide, H. *Polym. J.* **2008**, *40*, 763−767. (c) Nakamura, K.; Kanazawa, K.; Kobayashi, N. *Chem. Commun.* **2011**, *47*, 10064−10066.
(17) Koshika, K.; Chikushi, N.; Sano, N.; Oyaizu, K.; Nishide, H. *Green Chem.* **2010**, *12*, 1573−1575.
(18) (a) Kosower, E. W.; Cotter, J. L. *J. Am. Chem. Soc.* **1961**, *86*, 5524−5527. (b) Winters, L. J.; Borror, A. L.; Smith, N. G. *Tetrahedron Lett.* **1967**, *8*, 2313−2315. (c) Ageishi, K.; Endo, T.; Okawara, M. *J. Polym. Sci., Polym. Chem. Ed.* **1983**, *21*, 293−300. (d) Saika, T.; Iyoda, T. *Bull. Chem. Soc. Jpn.* **1993**, *66*, 2054−2060.
(19) (a) Kamata, K.; Kawai, T.; Iyoda, T. *Langmuir* **2001**, *17*, 155−163. (b) Kamata, K.; Suzuki, T.; Kawai, T.; Iyoda, T. *J. Electroanal. Chem.* **1999**, *473*, 145−155.
(20) (a) Nakamura, N.; Huang, H.; Qian, D. *Langmuir* **2002**, *18*, 5804−5809. (b) Creager, S. E.; Collard, D. M.; Fox, M. A. *Langmuir* **1990**, *6*, 1617−1620.
(21) (a) Laurent, D.; Schlenoff, J. B. *Langmuir* **1997**, *7463*, 1552−1557. (b) Zotti, G.; Zecchin, S.; Vercelli, B.; Berlin, A.; Grimoldi, S.; Bertoncello, R.; Milanese, L. *J. Electroanal. Chem.* **2005**, *580*, 330−339.
(22) Akahoshi, H.; Toshima, S.; Itaya, K. *J. Phys. Chem.* **1981**, *85*, 818−822.
(23) Hunter, T. B.; Tyler, P. S.; Smyrl, W. H.; White, H. S. *J. Electrochem. Soc.* **1987**, *134*, 2198−2204.
(24) Chikushi, N.; Yamada, H.; Oyaizu, K.; Nishide, H. *Sci. China Chem.* **2012**, *55*, 822−829.
(25) (a) Hoffman, A. S. *Adv. Drug Delivery Rev.* **2002**, *43*, 3−12. (b) Pal, K.; Banthia, A. K.; Majumdar, D. K. *Des. Monomers Polym.* **2009**, *12*, 197−220.